A Centralized Multilayer LPV/H∞ vs Decentralized Sliding Mode Control Architectures, for the Lane Keeping and Stability of an Intelligent Vehicle

Alex Hamdan, Reine Talj, Véronique Cherfaoui

A Centralized Multilayer $LPV/\mathscr{H}_\infty$ vs Decentralized Sliding Mode Control Architectures, for the Lane Keeping and Stability of an Intelligent Vehicle

Alex Hamdan * **Reine Talj** * **Véronique Cherfaoui** *

* *Sorbonne université, Université de technologie de Compiègne, CNRS, Heudiasyc UMR 7253, CS 60 319, 60 203 Compiègne, France (e-mail: alex.hamdan@hds.utc.fr).*

Abstract: This paper deals with the development of two Advanced Driving Assistance systems (*ADASs*) architectures involving the Active Front Steering (*AFS*) and the Direct Yaw Control (*DYC*) for the Lane Keeping and the lateral stability enhancement in Semi-Autonomous Vehicles. The objective of these systems is to assist and help the driver to keep the lane and to ensure lateral stability. To do that, a new Centralized and Decentralized architectures of *ADAS* system are developed. The different layers of each architecture are detailed including the control layer where the $LPV/\mathscr{H}_\infty$ and the Super-Twisting Sliding Mode (*STSM*) control techniques are used for the development of *ADAS* controllers respectively. Then, a decision making layer monitors the driver's behavior and the lateral stability to adjust the different controllers. Both *ADAS* system architectures are validated on Matlab/Simulink for a defined scenario with a complete nonlinear model of the vehicle validated on "*SCANeR Studio*" (OKtal) professional simulator. Finally, a comparison is done between them to show the difference in performance and the effectiveness of both strategies of control on the assistance objective and guaranteeing vehicle's stability.

Keywords: Semi-autonomous vehicle, *ADAS* systems, Centralized $LPV/\mathscr{H}_\infty$ control technique, Decentralized Sliding Mode control technique, Decision-making, Human-machine cooperative control.

1. INTRODUCTION

Active safety is an important issue that should be considered while driving on the road. In 2013, the US Department of Transportation "National Highway Traffic Safety Administration NHTSA" has classified the automation of vehicles into 5 levels to characterize their capabilities [Favarò et al. (2017)]. These levels start at having some assistance features and end at the full-autonomous vehicle passing by the semi-autonomous ones. Level 2 of automation consists of assisting the driver by several automated functionalities especially for active safety purpose. These systems are called Advanced Driving Assistance Systems (*ADASs*). They are integrated in the vehicle to protect the passengers in case of accident. There are the Passive systems (air bags, seat belts, etc.), and the Active systems that help and assist the driver in some driving tasks especially when he is tired or distracted (Lane keeping system, Emergency braking, Lane departure avoidance, etc.). In addition, many Advanced Driving Assistance System (*ADAS*) have been proposed and marketed, such as: Active Front Steering (*AFS*) basically to enhance vehicle's maneuverability; Direct Yaw Control (*DYC*) or Electronic Stability Program (*ESP*) to improve vehicle's lateral stability; Active Suspensions (*AS*) to improve comfort and rollover avoidance. These systems influence the vehicle's behavior and enhance safety on the road. Moreover, the development of electronics and sensors devices (LIDAR, GPS, etc.) supports the integration of these systems into the vehicle. The authors in Kukkala et al. (2018) classified the *ADAS* systems to many categories based on their types, utilities, limitations, etc. In addition, many advanced studies are presented in the literature to deal with the development of these systems especially the Lane Keeping system. A Fuzzy Takagi-Sugeno control method is used in Soualmi et al. (2011) to develop a lane keeping assistance system where a decision algorithm is integrated to manage the authority between the driver and the controller depending on the lateral deviation error. The authors in Nguyen et al. (2015) have developed a shared steering controller for lane keeping maneuver where the driver's activity and behavior are considered in the computation of the control input of assistance system, in order to manage conflict between both agents. An assistance steer-by-wire system is presented in Perozzi et al. (2020), where the fusion of two steering inputs is done considering the driver's availability via monitoring system. The authors in Sentouh et al. (2013) applied the H_2 approach to calculate the assistance torque through a first order filter coordination variable. A weighting approach presented in Borroni and Tanelli (2018) is used to blend the two control inputs by using a fusion parameter α adjusted manually or automatically depending on the driving situations. A similar approach is developed in Li et al. (2020) where the computation of α takes into consideration many factors: avoidance of lane departure, excessive steering, etc, to deal with lane following in case of tire blowout. Note that the main difference between the presented works cited above is how to determine the fusion parameter α in order to realize the assistance objective. All these interesting studies have motivated us to design new centralized and decentralized *ADAS* System architectures including the Active Front Steering (*AFS*) and the Direct Yaw Control (*DYC*) for the lane keeping purpose using steer-by-wire system and for the vehicle lateral stability improvement. However, this method can be adapted to overcome more complex maneuvers. Thus, in the present work, a new centralized $LPV/\mathscr{H}_\infty$ architecture of the *ADAS* System given in the Fig. 1, is developed to assist the driver in an intuitive way during a lane keeping maneuver while

guaranteeing vehicle's stability. The paper's contributions are as follows:

- A new centralized and decentralized *ADAS* System architectures by using: the $LPV/\mathscr{H}_\infty$ and the Super-Twisting Sliding Mode ($STSM$) control techniques respectively to stay within the lane and maintaining the lateral stability of the vehicle.
- A decision layer based on the driver's behavior and the lateral stability index for the adjustment of different controllers.
- A comparison between both *ADAS* architectures in terms of effectiveness and performance of each approach.

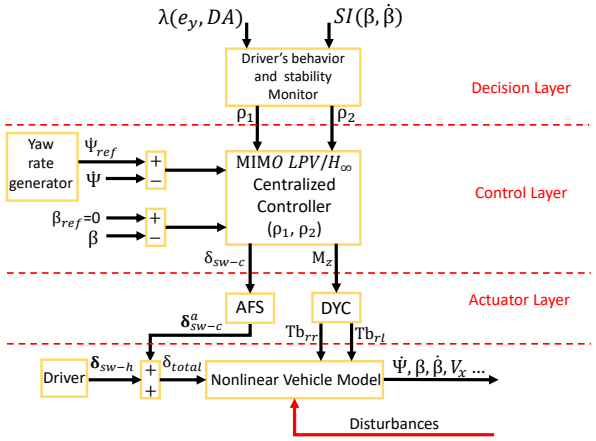

Fig. 1. Centralized $LPV/\mathscr{H}_\infty$ *ADAS* system architecture.

The paper structure is as follow: in Section 2 a vehicle bicycle model is given for the control synthesis. The centralized and decentralized *ADAS* system architectures including the different layers are detailed in the Sections 3 and 4 respectively. Then, in Section 5, the simulation results and validation for a given scenario are described to show the performance of both proposed *ADAS* systems. Finally, the conclusions and the perspectives for future work are given in Section 6.

2. CONTROL SYNTHESIS VEHICLE MODEL

The vehicle bicycle model used for control synthesis is a linear simplified LTI vehicle model. It is an LPV model with two variables being the vehicle side-slip angle β and the yaw rate $\dot{\psi}$. This model is used to develop the different controllers of this work and it is given by the following system:

$$Plant\ P: \begin{cases} \dot{\beta} = -\frac{C_f+C_r}{mV_x}\beta - (1+\frac{l_fC_f-l_rC_r}{mV_x^2})\dot{\psi} \\ \qquad\qquad +\frac{C_f}{mV_x}\delta_{sw-c}, \\ \ddot{\psi} = -\frac{l_fC_f-l_rC_r}{I_z}\beta - \frac{l_f^2C_f+l_r^2C_r}{I_zV_x}\dot{\psi} \\ \qquad\qquad +\frac{l_fC_f}{I_z}\delta_{sw-c}+\frac{1}{I_z}M_z, \end{cases} \quad (1)$$

where β and $\dot{\psi}$ are respectively the vehicle side-slip angle and the vehicle yaw rate. m is the vehicle mass, $l_{f,r}$ are the distances from the vehicle center of gravity to the front and rear axles respectively, $C_{f,r}$ are the front and rear tire cornering stiffness, I_z is the vehicle yaw moment of inertia, V_x is the vehicle longitudinal speed and finally δ_{sw-c} and M_z are the steering angle and the yaw moment representing the AFS and the DYC inputs respectively. The state space representation of the *Plant P* can be formalized as in (2), where $X=[\beta,\dot{\psi}]^T$ is the state vector, $U=[\delta_{sw-c},M_z]^T$ is the control input.

3. CENTRALIZED ARCHITECTURE

This section provides a full description of the centralized multilayer *ADAS* architecture given in the Fig. 1 based on the optimal $LPV/\mathscr{H}_\infty$ control technique. In the control layer, the output variables i.e the vehicle yaw rate $\dot{\psi}$ and the side-slip angle β are fed-back from the nonlinear Vehicle Model and are controlled/optimized together through an optimal Multi-Input-Multi-Output $MIMO\ LPV/\mathscr{H}_\infty$ controller, in order to realize a lane following trajectory (by controlling the vehicle yaw rate $\dot{\psi}$) while guaranteeing vehicle's lateral stability (by controlling the vehicle side-slip angle β). A yaw rate generator is used to generate the desired yaw rate $\dot{\psi}_{ref}$, and the desired side-slip angle is equal to 0 ($\beta_{ref}=0$) to enhance the lateral stability of the vehicle. In addition, two time-varying scheduling gains/parameters ρ_1 and ρ_2 schedule the two objectives of the $MIMO\ LPV/\mathscr{H}_\infty$ controller. Then, a decision layer (the higher layer) is developed to control the driving situation. It sends the value of the scheduling parameters, based on two criteria: 1) driver's behavior λ and 2) the lateral stability index (SI). So, based on all these information, the $MIMO\ LPV/\mathscr{H}_\infty$ controller generates the corrective control steering angle δ_{sw-c} provided by the AFS and the direct yaw moment M_z provided by the DYC as the control inputs. Finally, the actuators constraints are considered in the actuator layer.

3.1 Centralized Control Layer synthesis: $LPV/\mathscr{H}_\infty$ controller

Fig. 2 shows the control layer architecture. The standard $\mathscr{H}_\infty$ structure contains the controller $K_{LPV/\mathscr{H}_\infty}(\rho_1,\rho_2)$ to be synthesized, and the generalized plant $\sum_g$, where $\rho_1(\lambda)$ and $\rho_2(SI)$ are two weighted parameters calculated in the decision making layer, to adapt the controller dynamics and performances according to the driving conditions.

The errors between the desired trajectories and the actual ones of the yaw rate e_ψ (e_ψ=$\dot{\psi}_{ref}$-$\dot{\psi}$) and the side-slip angle e_β (e_β=β_{ref}-β) are the inputs to the controller $K_{LPV/\mathscr{H}_\infty}(\rho_1,\rho_2)$. Note that the $\mathscr{H}_\infty$ approach is a model-based robust control technique, then the actual yaw rate and the side-slip angle are calculated based on the LTI vehicle model of the Section 2 (*Plant P*).

The state representation of the *Plant P* of the generalized plant $\sum_g$ is formalized in (2), where $X=[\beta,\dot{\psi}]^T$ is the state vector, the actual yaw rate $\dot{\psi}$ and the side-slip angle β are also the outputs to be controlled, $U=[\delta_{sw-c},M_z]^T$ is the vector of control inputs.

The remaining subsystems of $\sum_g$ i.e. the weighting functions $W_{\dot{\psi}}(\rho_1)$, $W_\beta(\rho_2)$, $W_\delta(\rho_1)$, and $W_{M_z}(\rho_2)$ of Fig. 2 are defined to characterize the performance objectives Z_1, Z_2, and the actuators' constraints Z_3 and Z_4. The general form of these weights [Doumiati et al. (2014)] is given as:

- $W_{\dot{\psi}}(\rho_1)$ weights the yaw rate control objective:

$$W_{\dot{\psi}}(\rho_1) = \rho_1\frac{s/M_1+2\pi f_1}{s+2\pi f_1A_1}, \quad (3)$$

where M_1 is sufficiently high for a large robustness margin, and A_1 is the tolerated tracking error on e_ψ. $W_{\dot{\psi}}(\rho_1)$ is used to reduce the yaw rate error. $W_{\dot{\psi}}(\rho_1)$ is linearly parametrized by the varying parameter ρ_1, where $\rho_1 \in \left\{\underline{\rho_1} \le \rho_1 \le \overline{\rho_1}\right\}$ ($\underline{\rho_1}$ and $\overline{\rho_1}$ are constants representing the lower and higher values of ρ_1). When $\rho_1=\overline{\rho_1}$, the performance objective $e_{\dot{\psi}}$ is prioritized and the *ADAS* system (AFS) is switched-on; on the contrary, when $\rho_1=\underline{\rho_1}$, $e_{\dot{\psi}}$ is relaxed, so the driver navigates correctly and the

$$\dot{X} = \begin{bmatrix} \dot{\beta} \\ \ddot{\psi} \end{bmatrix} = \underbrace{\begin{bmatrix} -\frac{C_f+C_r}{mV_x} & -(1+\frac{l_fC_f-l_rC_r}{mV_x^2}) \\ -\frac{l_fC_f-l_rC_r}{I_z} & -\frac{l_f^2C_f+l_r^2C_r}{I_zV_x} \end{bmatrix}}_{A} \begin{bmatrix} \beta \\ \dot{\psi} \end{bmatrix} + \underbrace{\begin{bmatrix} \frac{C_f}{mV_x} & 0 \\ \frac{l_fC_f}{I_z} & \frac{1}{I_z} \end{bmatrix}}_{B} \begin{bmatrix} \delta_{sw-c} \\ M_z \end{bmatrix} \tag{2}$$

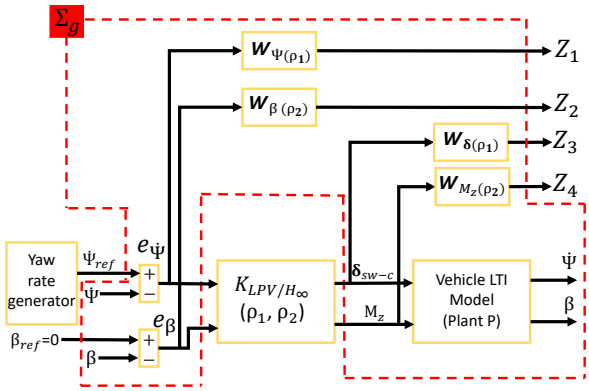

Fig. 2. Control layer architecture.

ADAS system (*AFS*) for trajectory following is switched-off.
- $W_\beta(\rho_2)$ weights the side-slip angle control objective:

$$W_\beta(\rho_2) = \frac{1}{\rho_2}\frac{s/M_2+2\pi f_2}{s+2\pi f_2 A_2}. \tag{4}$$

where M_2, A_2 and f_2 have similar meanings as M_1, A_1 and f_1. $W_\beta(\rho_2)$ is similar to $W_\psi(\rho_1)$. The main difference is that $W_\beta(\rho_2)$ is inversely dependent on the varying parameter ρ_2. This is because ρ_2 is inversely related to the lateral stability index *SI*, that means the lateral stability is prioritized when $\rho_2 = \underline{\rho_2}$ and vice-versa. This issue is explained later in the decision layer.
- $W_\delta(\rho_1)$ weights the steering control input, δ_{sw-c}:

$$W_\delta(\rho_1) = \frac{1}{\rho_1}\frac{s+2\pi f_3/M_3}{\varepsilon_u s+2\pi f_3}, \tag{5}$$

where M_3 is sufficiently high for a large robustness margin, ε_u is concerned with the noise rejection at high frequencies and f_3 is the filter's frequency. This filter forces the steering system to act at this frequency in order to avoid driver annoyance. This filter design is inspired from Atoui et al. (2021). $W_\delta(\rho_1)$ depends on ρ_1, which allows to promote or penalize the steering depending on all possible situations. For instance, when driver's behavior is wrong, *AFS* is promoted to realize the lane keeping (when $\rho_1 = \overline{\rho_1}$) and help the driver. However, if the driver acts appropriately, *AFS* is penalized (relaxed) (when $\rho_1 = \underline{\rho_1}$) and in this case, the driver is the only responsible of driving action.
- $W_{M_z}(\rho_2)$ weights the braking control input, M_z:

$$W_{M_z}(\rho_2) = \rho_2 10^{-3}\frac{s/(2\pi f_4)+1}{s/(\kappa 2\pi f_4)+1}, \tag{6}$$

where f_4 is the braking actuator cut-off frequency and κ to handle the braking actuator limitations (see Doumiati et al. (2013)). When $\rho_2 = \underline{\rho_2}$, the braking control signal is promoted, on the contrary, when $\rho_2 = \overline{\rho_2}$, the braking input is penalized. This filter is designed depending on the vehicle's lateral stability.
After determining the subsystems of Fig. 2, the $LPV/\mathscr{H}_\infty$ control technique is applied to minimize the controlled outputs Z_1, Z_2, Z_3 and Z_4 of the generalized plant $\sum_g$ for any exogenous input. More information about the optimal $LPV/\mathscr{H}_\infty$ theory is given in Sename et al. (2013).
The Matlab function "*sysic*" (Robust Control Toolbox) interconnects the subsystems of $\sum_g$. Remember that $\sum_g$ is a *LPV* [Apkarian et al. (1995)] formulated as:

$$\Sigma_g(\rho): \begin{bmatrix} \dot{x} \\ z \\ y \end{bmatrix} = \begin{bmatrix} A(\rho) & B_1(\rho) & B_2(\rho) \\ C_1(\rho) & D_{11}(\rho) & D_{12}(\rho) \\ C_2 & D_{21} & 0 \end{bmatrix} \begin{bmatrix} x \\ w \\ U \end{bmatrix}, \tag{7}$$

where $\rho = \{\rho_1, \rho_2\}$, x includes the state variables of *Plant P* and the weighting functions, $w = [\psi_{ref}, \beta_{ref}]^T$ is the exogenous input vector representing the reference of the outputs, $U = [\delta_{sw-c}, M_z]^T$ represents the control inputs, $y = [\psi, \beta]^T$ is the measurement vector fed-back to the controller, and $z = [Z_1, Z_2, Z_3, Z_4]^T$ is the weighted controlled output vector.
Note that the matrices B_2, and D_{12} depend on ρ, which is not compatible with $\mathscr{H}_\infty$ requirements for polytopic systems. However, this problem is solved using some filter on the control input [Apkarian and Gahinet (1995)].
***Problem resolution:** LMI based $LPV/\mathscr{H}_\infty$:*
The *LMI* based $LPV/\mathscr{H}_\infty$ problem consists in finding the controller $K_{LPV/\mathscr{H}_\infty}(\rho_1, \rho_2)$, in order to minimize the $\mathscr{H}_\infty$ norm of the closed-loop *LPV* system formed by the equations (7) and (8). Note that the controller $K_{LPV/\mathscr{H}_\infty}(\rho_1, \rho_2)$ is given as:

$$K_{LPV/\mathscr{H}_\infty}(\rho_1, \rho_2): \begin{bmatrix} \dot{x}_c \\ u \end{bmatrix} = \begin{bmatrix} A_c(\rho) & B_c(\rho) \\ C_c(\rho) & 0 \end{bmatrix} \begin{bmatrix} x_c \\ y \end{bmatrix}, \tag{8}$$

Many approaches exist in the literature to solve this problem such as: polytopic, gridding and Linear Fractional Transformation *LFT* [Zin (2005)]. In the present work, a polytopic approach (see Scherer et al. (1997)) has been used for controller synthesis. Using the Bounded Real Lemma (*BRL*) extended to *LPV* systems and after a change of basis presented in Scherer et al. (1997), a non conservative *LMI* is formulated in (9) and a Semi-Definite Program (*SDP*) has been applied to solve these inequalities equations (see [Doumiati et al. (2013)]), while minimizing γ for $\rho \in \Omega = [\underline{\rho_1}, \overline{\rho_1}]\mathrm{x}[\underline{\rho_2}, \overline{\rho_2}]$.
The polytopic approach aims to find the $\widetilde{A}(\rho)$, $\widetilde{B}(\rho)$ and $\widetilde{C}(\rho)$ by using a common Lyapunov function i.e $X(\rho) > 0$ and $Y(\rho) > 0$ at each vertex of the polytope function of $\rho \in \Omega$. Noting that the number of vertex is 4 (2^n) where n is the number of parameters ρ_i. Thus, the solution is given by the resolution of system (10) at each vertex of the convex hull Ω $\left\{\omega_1 = (\underline{\rho_1}, \underline{\rho_2}), \omega_2 = (\overline{\rho_1}, \underline{\rho_2}), \omega_3 = (\underline{\rho_1}, \overline{\rho_2}), \omega_4 = (\overline{\rho_1}, \overline{\rho_2})\right\}$:

$$\begin{cases} C_c(\rho) = \widetilde{C}(\rho)M(\rho)^{-T} \\ B_c(\rho) = N(\rho)^{-1}\widetilde{B}(\rho) \\ A_c(\rho) = N(\rho)^{-1}(\widetilde{A}(\rho) - Y(\rho)A(\rho)X(\rho) - N(\rho)B_c(\rho)C_2X(\rho) \\ \qquad - Y(\rho)B_2(\rho)C_c(\rho)M(\rho)^{-T})M(\rho)^{-T} \end{cases}, \tag{10}$$

where $M(\rho)N(\rho)^T = I - X(\rho)Y(\rho)$ with $M(\rho)$ and $N(\rho)$ are given by the user. More details about the computation solution have been presented in Scherer et al. (1997). Referring to the polytopic approach, the final controller $K_{LPV/\mathscr{H}_\infty}(\rho_1, \rho_2)$ is the weighted summation of each convex controller calculated on each vertex of the polytope [Apkarian et al. (1995)] such as:

$$\begin{aligned} K_{LPV/\mathscr{H}_\infty}(\rho_1, \rho_2) = \alpha_1 K_{\mathscr{H}_\infty}(\omega_1) + \alpha_2 K_{\mathscr{H}_\infty}(\omega_2) \\ + \alpha_3 K_{\mathscr{H}_\infty}(\omega_3) + \alpha_4 K_{\mathscr{H}_\infty}(\omega_4), \end{aligned} \tag{11}$$

$$\begin{bmatrix} A(\rho)X + XA(\rho)^T + B_2\widetilde{C}(\rho) + \widetilde{C}(\rho)^T B_2^T & (*)^T & (*)^T & (*)^T \\ \widetilde{A}(\rho) + A(\rho)^T & YA(\rho) + A(\rho)^T Y + \widetilde{B}(\rho)C_2 + C_2^T \widetilde{B}(\rho)^T & (*)^T & (*)^T \\ B_1(\rho)^T & B_1(\rho)^T Y + D_{21}^T \widetilde{B}(\rho)^T & -\gamma I & (*)^T \\ C_1(\rho)X + D_{12}\widetilde{C}(\rho) & C_1(\rho) & D_{11}(\rho) & -\gamma I \end{bmatrix} < 0 \text{ and } \begin{bmatrix} X(\rho) & I \\ I & Y(\rho) \end{bmatrix} > 0. \tag{9}$$

where $\sum_{i=1}^{i=4} \alpha_i(\rho_1,\rho_2) = 1$; $\alpha_i(\rho_1,\rho_2) > 0$. Depending on the driving situation given in Fig. 3, the different polytopic coordinates $\alpha_i(\rho_1,\rho_2)$ weight the controller on each vertex where each vertex represents an objective, in order to build the final controller of our system. They are calculated by using the Matlab function"*polydec*" (Robust Control Toolbox):

$$\begin{aligned} \alpha_1 &= \frac{\overline{\rho_1}-\rho_1}{\overline{\rho_1}-\underline{\rho_1}}.\frac{\overline{\rho_2}-\rho_2}{\overline{\rho_2}-\underline{\rho_2}}; \quad & \alpha_3 &= \frac{\overline{\rho_1}-\rho_1}{\overline{\rho_1}-\underline{\rho_1}}.\frac{\rho_2-\underline{\rho_2}}{\overline{\rho_2}-\underline{\rho_2}}; \\ \alpha_2 &= \frac{\rho_1-\underline{\rho_1}}{\overline{\rho_1}-\underline{\rho_1}}.\frac{\overline{\rho_2}-\rho_2}{\overline{\rho_2}-\underline{\rho_2}}; \quad & \alpha_4 &= \frac{\rho_1-\underline{\rho_1}}{\overline{\rho_1}-\underline{\rho_1}}.\frac{\rho_2-\underline{\rho_2}}{\overline{\rho_2}-\underline{\rho_2}}. \end{aligned} \tag{12}$$

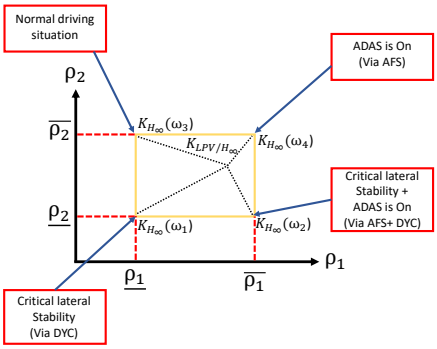

Fig. 3. Polytopic $\mathscr{H}_\infty$ controller

Yaw rate generator at a look-ahead distance:
The reference yaw rate generator is developed at a look-ahead distance l_s in front of the vehicle, in order to generate a coherent reference yaw rate $\dot{\psi}_{ref}$ to the *MIMO LPV*$/\mathscr{H}_\infty$ controller for the trajectory following purpose. This controller aims that $\dot{\psi}$ follows $\dot{\psi}_{ref}$ in order to keep the lane with a high accuracy. For that, the reference yaw rate generator uses the current vehicle's speed V_x and the information from the map matching e_{y-l_s} to calculate $\dot{\psi}_{ref}$. Refer to Tan and Huang (2014), $\dot{\psi}_{ref}$ can be approximated as:

$$\dot{\psi}_{ref} = \frac{-2V_x e_{y-l_s}}{l_s^2} \tag{13}$$

where e_{y-l_s} is the vehicle lateral error at a look-ahead distance l_s.

3.2 Decision Layer: ρ_1 and ρ_2 calculations

The decision layer is developed to monitor the controller according to the driving situations. This layer delivers the scheduling parameters ρ_1 and ρ_2 depending on the driver's behavior (λ) and the lateral stability index (*SI*) respectively. Before the calculation of ρ_1 and ρ_2, let us introduce the definition of both criteria λ and *SI* of this layer.

Driver's behavior λ:
λ is function of the lateral error e_y of the vehicle w.r.t the trajectory at the center of gravity of the vehicle (*CG*) and the driver's availability (*DA*). $DA \in [0,1]$ is a dynamic variable related to the driver. *DA*=1 corresponds to a full driver's confidence. It can be calculated based on different factors: driver's eyes analysis, driver's head position, level of driver's sleepiness, etc. Therefore, the calculation of diver's availability is not in the scope of this work and it is considered as an input given by a diagnosis module to this layer. λ is expressed as:

$$\lambda = |e_y| + (1 - DA) \tag{14}$$

λ has two rules depending on e_y and *DA*, given as follows:
* When $\lambda \leq \underline{\lambda}$, that means $|e_y| \leq \underline{e_y}$ and *DA*=1, the *ADAS* system *AFS* is switched-off (no need to assistance).
* When $\lambda \geq \overline{\lambda}$, that means $|e_y| \geq \overline{e_y}$ and/or *DA* is simply low (*DA*=0), so the *ADAS* system *AFS* should be switched-on, in order to compensate the driver's error and unavailability.
According to this analysis, the scheduled gain ρ_1 feeds the *LPV*$/\mathscr{H}_\infty$ controller the sufficient information about the weights to be pushed or attenuated. The relation between ρ_1 and λ is presented by a "*sigmoid*" function (15) (see Fig. 4).

$$\rho_1 = \underline{\rho_1} + \frac{\overline{\rho_1} - \underline{\rho_1}}{1 + e^{-\frac{8}{\overline{\lambda}-\underline{\lambda}}(\lambda - \frac{\overline{\lambda}+\underline{\lambda}}{2})}} \tag{15}$$

For the ρ_2 calculation, ρ_2 depends on the lateral stability indicator *SI*.

Lateral stability index SI:
The Lateral stability index *SI* reflects the orientation of the vehicle depending on the speed vector at the center of gravity *CG*, and its rate of change. *SI* is given as (see Hamdan et al. (2020)):

$$SI = \left| c_1\beta + c_2\dot{\beta} \right|, \tag{16}$$

where c_1 and c_2 are estimated w.r.t the vehicle parameters and the shape of the road. *SI* is between 0 and 1 in stable driving. *SI* determines the driving situations. *SI* has two rules:
* When $SI \leq \underline{SI}$ (a predefined lower threshold depending on the road's parameters and vehicle), the vehicle is in normal driving situation (stable region) and *ADAS* system for stability (*DYC*) is penalized (not needed).
* when $SI \geq \overline{SI}$ (a predefined higher threshold), the vehicle is in critical lateral stability region (unstable region) and a stability *ADAS* system *DYC* is needed to be triggered to reestablish the lateral stability of the vehicle.
According to this discussion, ρ_2 is calculated based on the *SI* in order to provide the *LPV*$/\mathscr{H}_\infty$ controller information about the weights to be pushed or attenuated. The relation between ρ_2 and *SI* is given through a "*sigmoid*" function (17) (see Fig. 4) that guarantees a continuous and smooth variation of ρ_2.

$$\rho_2 = \overline{\rho_2} - \frac{\overline{\rho_2} - \underline{\rho_2}}{1 + e^{-\frac{8}{\overline{SI}-\underline{SI}}(SI - \frac{\overline{SI}+\underline{SI}}{2})}}; \tag{17}$$

3.3 Actuator Layer:

The Actuator Layer contains the two actuators *AFS* and the *DYC* used to generate the physical control inputs of the system. The *AFS* is an electrical motor which provides the added steering angle δ^a_{sw-c}. In order to ensure that the *AFS* actuator

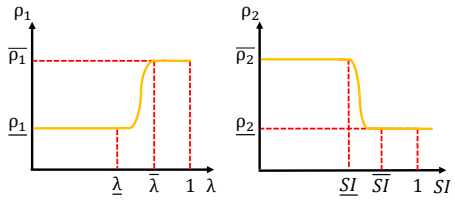

Fig. 4. Scheduling parameters ρ_1 and ρ_2

is able to provide the added steering angle demanded by the controller δ_{sw-c}, the AFS is modeled as follows:

$$\dot{\delta}^a_{sw-c} = 2\pi f_3(\delta_{sw-c} - \delta^a_{sw-c}) \tag{18}$$

where δ^a_{sw-c} follows δ_{sw-c}, f_3 is the actuator cut-off frequency. This actuator is bounded between $\left[-\delta^a_{sw-c,max}, +\delta^a_{sw-c,max}\right]$, with $\delta^a_{sw-c,max}$ the maximum amount of steering angle that can be added by the AFS actuator for assistance purpose. Note that the total steering wheel angle is given as: $\delta_{total} = \delta_{sw-h} + \delta^a_{sw-c}$, where ρ_1 is implicitly expressed in δ^a_{sw-c}. δ_{sw-h} is the human's steering angle, representing the human driver in-the-loop, delivered by the developed Driver Model in Hamdan et al. (2021).

Concerning the DYC actuator, the DYC moment M_z can be realized by applying on the low-level a differential braking torque on one rear wheel (left or right) of radius r [Hamdan et al. (2020)]. The applied braking torque is given as follows:

$$\begin{cases} \begin{cases} Tb_{rr} = -\frac{2*M_z*r}{t_r}, \\ Tb_{lr} = 0, \end{cases} & if\ M_z \leq 0, \\ \begin{cases} Tb_{lr} = \frac{2*M_z*r}{t_r}, \\ Tb_{rr} = 0, \end{cases} & if\ M_z > 0, \end{cases} \tag{19}$$

where Tb_{lr} and Tb_{rr} are the left and right differential braking torques respectively. A simple model for the electro mechanical braking (EMB) actuator is used. The EMB actuator is modeled as:

$$\dot{T}^a_{b,rj} = 2\pi f_4(T_{b,rj} - T^a_{b,rj}), \tag{20}$$

where $T^a_{b,rj}$ follows $T_{b,rj}$, f_4 is the actuator cut-off frequency. This actuator control is bounded between $[0, T^a_{b,max}]$, where $T^a_{b,max}$ is the saturation of the EMB actuator.

4. DECENTRALIZED ARCHITECTURE

In the decentralized approach, we decoupled the two objectives (trajectory tracking and vehicle's stability improvement) into two sub-control problems. The $STSM$ control technique is applied to provide the control inputs, such as: AFS is responsible on the control of the lateral error (e_y) in order to follow the trajectory; DYC is responsible on the control of side-slip angle (β) to enhance stability. The global decentralized multilayer control architecture is shown in Fig. 5. The main difference w.r.t the centralized one is in the control layer, where each controller generates his input by neglecting the other. The inputs are: AFS control input δ_{sw-c} dedicated to minimize the lateral error (e_y) in order to follow the trajectory, and DYC control input M_z devoted to control the side-slip angle β to improve vehicle's stability. However, the decision and actuator layers are similar to the ones of the centralized approach, where the decision layer generates the two weights, called α and γ in this case; function of λ and SI respectively. The aim of these gains is to promote/attenuate both $STSM$ controllers depending on driver's behavior (λ) and the lateral stability indicator (SI).

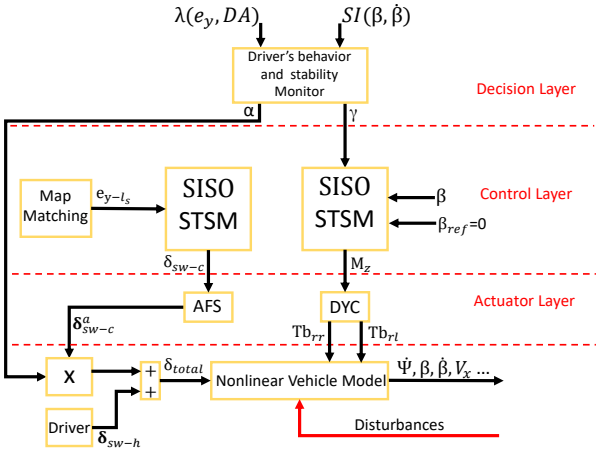

Fig. 5. Decentralized $STSM$ $ADAS$ system architecture.

4.1 Decentralized Control Layer synthesis: Super-twisting sliding mode controllers

The control layer consists of two Single-Input-Single-Output $SISO$ $STSM$ controllers generating the control inputs. For that, the $STSM$ control technique detailed in Hamdan et al. (2021) is used here to find the control inputs: δ_{sw-c} and M_z. The AFS provides the δ_{sw-c} to minimize the lateral error e_y (defined later) and realize the path following. The DYC generates the yaw moment M_z to control the side-slip angle β and enhance the vehicle's lateral stability. The longitudinal movement for both architectures is realized also using a STSM controller developed in Hamdan et al. (2021).

The $STSM$-based AFS control synthesis model is similar to (2), while considering $M_z = 0$, and thus, reducing B to its first column B_1. The driver steering input δ_{sw-h} is neglected in the synthesis model and it is fed-forward to the system.

The $STSM$-based DYC control synthesis model is similar to (2), while considering $\delta_{sw-c} = 0$, and thus, reducing B to its second column B_2. The driver steering input δ_{sw-h} is also neglected in the synthesis model.

Let's recall the second order system given as:

$$\dot{X} = f(X,t) + g(X,t)u(t) \tag{21}$$

where $X = [e_y, \beta]^T$, and $f(X,t) = AX$. In the case of the AFS controller synthesis $g(X,t) = B_1$ and $u = \delta_{sw-c}$. In the case of the DYC controller synthesis $g(X,t) = B_2$ and $u = M_z$.

Let's define $E = [e_y, e_\beta] = [y - y^*, \beta_{ref} - \beta]^T$ the error vector between the actual and the desired states. y^* and $\beta_{ref} = 0$ are the desired lateral coordinate of the road and the desired side-slip angle respectively. e_y is calculated by a Map Matching block at a look-ahead distance l_s, that localizes the vehicle on the reference map.

Let's define the two sliding variables for the two controllers as follows:

$$\begin{aligned} s_{e_y} &= \dot{e_y} + \lambda_y e_y, \quad \lambda_y > 0 \\ s_\beta &= \gamma(e_\beta + \lambda_\beta \dot{e_\beta}) \quad \lambda_\beta > 0 \end{aligned} \tag{22}$$

where λ_y and λ_β are positive constants. The sliding variables s_{e_y} and s_β have a relative degree equal to one w.r.t the control inputs δ_{sw-c} (for the lateral dynamics) and M_z respectively, since B_1 and B_2 are not zero, as can be seen in the control synthesis model (2). $\gamma_{(SI)}$ is a scheduling gain which varies between 0 and 1, provided by the decision layer discussed later. When $\gamma_{(SI)}$ is equal to 1, the DYC controller is promoted. When $\gamma_{(SI)}$ is equal to 0, the DYC controller is attenuated.

Thus, in order to achieve the convergence of the sliding variables to the sliding surface defined by $s = 0$ and based on the discussion in Hamdan et al. (2021), the *STSM* control inputs of the *AFS* and the *DYC* are respectively given by:

$$\delta_{sw-c} = -\alpha_{\delta,1}|s_{\psi,\theta}|^{\tau_\delta} sign(s_{\psi,\theta}) - \alpha_{\delta,2}\int_0^t sign(s_{\psi,\theta})d\tau,$$
$$M_z = -\alpha_{M_z,1}|s_\beta|^{\tau_{M_z}} sign(s_\beta) - \alpha_{M_z,2}\int_0^t sign(s_\beta)d\tau, \quad (23)$$

where $\alpha_{\delta,1}$ and $\alpha_{\delta,2}$ (resp. $\alpha_{M_z,1}$ and $\alpha_{M_z,2}$) are positive gains. τ_δ and τ_{M_z} are constants in $]0,\ 0.5]$. The function *sign* is smoothed by the approximation $sign(s) = \frac{s}{|s|+\varepsilon}$, where ε is a positive small value. The *STSM* control inputs guarantee the convergence of s_{e_y} and s_β in a finite time to zero. Once $s_{e_y} = 0$ and $s_\beta = 0$, this means that y will converge to y^* and the side-slip angle β will converge to β_{ref} respectively.

Similar to the centralized approach, a decision layer of the decentralized approach monitors all the control objectives based on some monitoring criteria: λ and *SI*. Then, it calculates and sends instantly the values of α and γ to relax/promote the corresponding control objective depending on the vehicle situation.

α depends on the driver's behavior λ.

* When $\lambda \leq \underline{\lambda}$, that means $|e_y| \leq \underline{e_y}$ and *DA*=1, α approaches to 0 and the *ADAS* system *AFS* is attenuated.

* When $\lambda \geq \overline{\lambda}$, that means $|e_y| \geq \overline{e_y}$ and/or *DA*=0, α approaches to 1 so the *ADAS* system *AFS* should be promoted to assist the driver.

By the same way, γ depends on the lateral stability index *SI*.

* When $SI \leq \underline{SI}$, γ approaches to 0 since no lateral stability risk and the *ADAS* system *DYC* is penalized .

* When $SI \geq \overline{SI}$, γ approaches to 1 since the lateral stability risk is high and the *ADAS* system *DYC* is activated.

"*Sigmoid*" functions (24) (see Fig. 6) govern the relation between α and λ and between γ and *SI* respectively, to ensure a continuous and smooth variation of α and γ. Concerning the actuator layer, it is the same as the centralized architecture. Note that the final steering wheel angle is given as: $\delta_{total} = \delta_{sw-h} + \alpha * \delta^a_{sw-c}$ (see Fig. 5).

$$\alpha = \frac{1}{1+e^{-\frac{8}{\overline{\lambda}-\underline{\lambda}}(\lambda-\frac{\overline{\lambda}+\underline{\lambda}}{2})}}; \gamma = \frac{1}{1+e^{-\frac{8}{\overline{SI}-\underline{SI}}(SI-\frac{\overline{SI}+\underline{SI}}{2})}} \quad (24)$$

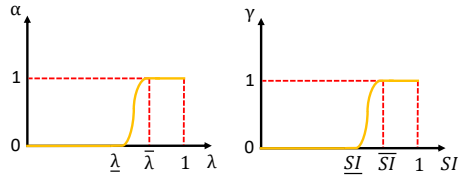

Fig. 6. Scheduling gains α and γ

5. SYSTEM'S VALIDATION

The proposed centralized *MIMO LPV*$/\mathscr{H}_\infty$ and the decentralized *STSM ADAS* system architectures are validated in this section. Validation is done by simulation using Matlab/Simulink with a complete nonlinear model of the vehicle, validated on "*SCANeR Studio*" (OKtal) simulator. Then, a comparison is done by integrating the proposed both architectures into the vehicle, and comparing it to a vehicle without *ADAS*, where the controllers are not implemented (driving without *ADAS*) in order to show the difference in terms of performance and effectiveness of each control technique. The different parameters numerical values of the two controllers used during the simulation are given in Table 1.

Table 1. Controllers' Parameters for Simulation

Parameters	Values
$M_1 = M_2; M_3; A_1 = A_2; \varepsilon_u; \kappa$	$2; 1; 0.1 = 10\%; 0.01; 100$
$f_1 = f_2; f_3 = f_4$	$11.15\ Hz; 10\ Hz$
$c_1; c_2; l_s; r; t_r; \lambda_y; \lambda_\beta; \varepsilon$	$9.55; 2.49; 3; 0.3; 0.75; 8; 0.1; 1$
$\underline{e_y}; \overline{e_y}; \underline{\lambda}; \overline{\lambda}; \underline{SI}; \overline{SI}; \underline{\rho_1}; \overline{\rho_1}; \underline{\rho_2}; \overline{\rho_2}$	$0.5; 0.7; 0.5; 0.7; 0.6; 0.7; 0.01; 1; 0.45; 10$
$\alpha_{\delta,1}; \alpha_{M_z,1}; \tau_\delta = \tau_{M_z}; \alpha_{\delta,2}; \alpha_{M_z,2}$	$0.1; 1000; 0.5; 0.01; 0.1$
$\delta^a_{sw-c,max}; T^a_{b,max}$	$5°; 1200\ N.m$

5.1 Simulation results

As mentioned before, this section is dedicated to validate and compare the proposed centralized *MIMO LPV*$/\mathscr{H}_\infty$ and the decentralized *STSM* architectures. A scenario is defined using the track given in the Fig. 7 to test and validate the proposed controllers which aim to assist the driver in the lane keeping maneuver at speed 60 Km/h (see Fig. 13), and improve the vehicle's stability, when needed, based on the decision monitoring. To do that, two errors are injected between $35s$ and $50s$ and between $70s$ and $85s$ on the driver's behavior, where he is no more available. The vehicle is deviated from the lane and the *ADAS* system (represented by the centralized or decentralized controller) is activated to diminish the driver's error (through *AFS*) and retain the lateral stability of the vehicle (through *DYC*). The simulation results show the importance of having an *ADAS* system in the vehicle, compensating driver's error and enhancing vehicle's stability. During this scenario, a comparison is done between the vehicle without *ADAS* (where driver is alone), and the proposed architectures i.e the driving with *ADAS LPV*$/\mathscr{H}_\infty$ centralized and the driving with *ADAS STSM* decentralized controllers.

The Fig. 8 shows the lateral error of: driver without *ADAS*, driving with *ADAS-LPV*$/\mathscr{H}_\infty$-centralized and driving with *ADAS-STSM*-decentralized. As we can see, the errors are injected on the driver's behavior between $35s$ and $50s$ and between $70s$ and $85s$. Both ADAS systems (*LPV*$/\mathscr{H}_\infty$ and *STSM* controllers) diminish this error (initially $1m$) caused by the driver on the curvy road (see Fig. 13). Thus, the two controllers have achieved the assistance goal with acceptable accuracy of lane keeping (e_y

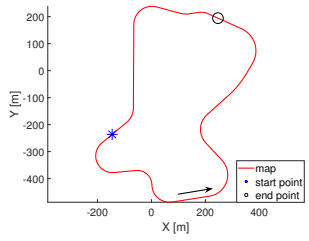

Fig. 7. Map of the tracked trajectory

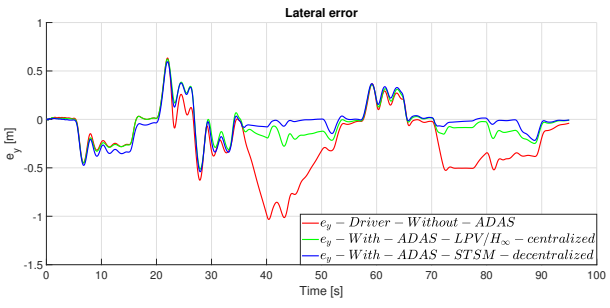

Fig. 8. The lateral error

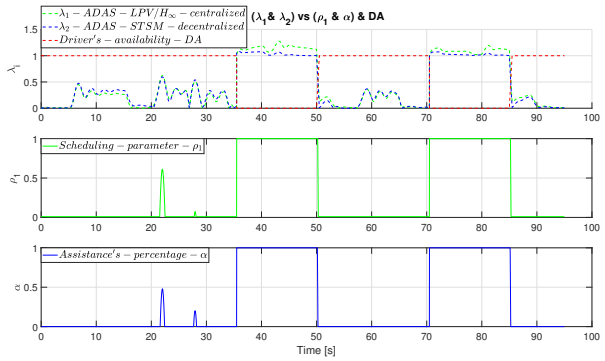

Fig. 9. λ_i vs ρ and α

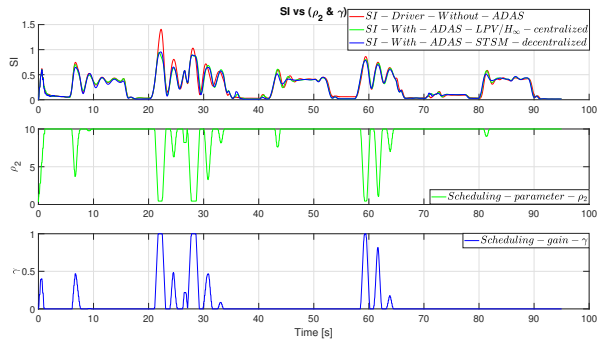

Fig. 10. SI vs ρ_2 and γ

between $-60cm$ and $60cm$, Fig. 8). However, Fig. 8 shows that the *ADAS-STSM*-decentralized controller is capable to diminish more the lateral error e_y to zero compared to the *ADAS-LPV*$/\mathscr{H}_\infty$-centralized controller that is less performant, because the *SISO STSM-AFS* controller realizes the lane keeping objective independently of *SISO STSM-DYC* controller (see Fig. 5). The two *ADAS* controllers are switched-on until t=50s, where $\lambda_i \geq \overline{\lambda}$ $(i = \{1 : ADAS - LPV/\mathscr{H}_\infty - centralized, 2 : ADAS - STSM - decentralized\})$ because the driver's availability *DA* is equal to 0 and the lateral error is more than $\overline{e_y}$ (see Fig. 9). Remember that *DA* reflects the driver's status (1 for available or 0 for not available). Again at t=70s, an *ADAS* controller is still needed because there is a second error caused by the driver's behavior and *DA*=0. The ADAS controllers assist the driver until t=85s. At t=85s, the driver's behavior returns normal and *DA*=1, then the two *ADAS* controllers are switched-off.

The switching-on of the two $ADAS - AFS$ controllers can be explained by observing the decision layer of each *ADAS* system architecture, in other words, the monitoring criterion λ_1 and λ_2. Fig. 9 shows the two parameters λ_1 and λ_2, with the corresponding scheduling parameter ρ_1 of the *LPV*$/\mathscr{H}_\infty$-centralized, and the percentage of assistance α of the *STSM*-decentralized *ADAS* system architecture, and, the driver's availability *DA*. For $\lambda_1 \geq \overline{\lambda}$ (resp. $\lambda_2 \geq \overline{\lambda}$), this means that the driver lost control and the two $ADAS - AFS$ controllers have switched-on to assist and help him. When $\lambda_1 \geq \overline{\lambda}$ (resp. $\lambda_2 \geq \overline{\lambda}$), that means $DA = 0$ and/or e_y is more than $\overline{e_y}$, especially between 35s and 50s and between 70s and 85s, the scheduling gain ρ_1 of the *LPV*$/\mathscr{H}_\infty$-centralized controller (resp. the percentage of assistance α of the *STSM*-decentralized controller) is set to $\rho_1 = \overline{\rho_1}$ (resp. $\alpha = 1$), which activates the assistance. For the region, when $\lambda_1 \leq \underline{\lambda}$ (resp. $\lambda_2 \leq \underline{\lambda}$), the scheduling gain ρ_1 (resp. the percentage of assistance α) is set to $\rho_1 = \underline{\rho_1}$ (resp. $\alpha = 0$), which means the driver acts correctly and the $ADAS - AFS$ controllers are switched-off. Thus, both $ADAS - AFS$ controllers have almost the same behavior and they are able to help the driver by compensating his errors.

On the other hand, both control architectures have similar influence on the lateral stability index *SI* as shown in the Fig. 10. The vehicle's lateral stability objective is achieved by the two controllers in order to prevent an undesirable driving situation ($SI > 1$). Fig. 10 shows the lateral *SI* with the corresponding scheduling parameter ρ_2 and the scheduling gain γ of both control architectures. The lateral index *SI* of the vehicle without *ADAS* (driver without *ADAS*) exceeds $SI = 1$, which means that the vehicle has lost its stability, while both control architectures have covered back the *SI* under $SI = \underline{SI}$, and thus, they have succeeded to remain the vehicle stable during the

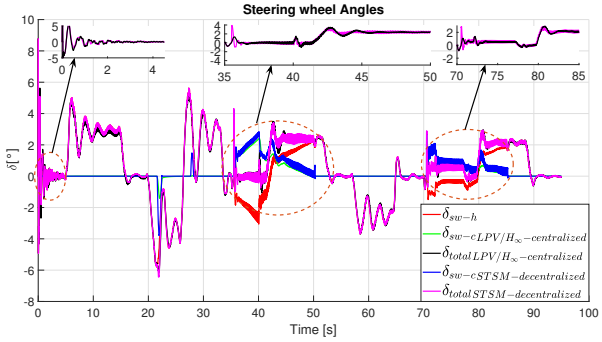

Fig. 11. The different total steering wheel angles

overall trajectory. Therefore, ρ_2 is chosen as $\rho_2 = \underline{\rho_2}$ (resp. γ is chosen as $\gamma = 1$) when $SI \geq \overline{SI}$ for the lateral stability enhancement through the activation of the differential braking actuator (*DYC*). When $SI \leq \underline{SI}$, ρ_2 (resp. γ) deviates to $\rho_2 = \overline{\rho_2}$ (resp $\gamma = 0$) which means the deactivation of the differential braking actuator (*DYC*), and there is no risk of lateral stability. Concerning the centralized *LPV*$/\mathscr{H}_\infty$ *ADAS* system control architecture, the choice and the tuning of the parameters ρ_1 and ρ_2 (Fig. 1) is not obvious since the *LPV*$/\mathscr{H}_\infty$ controller aims to compromise between the different control objectives in order to give an optimal result. Many simulations with tuning of these parameters are done to get the optimal one.

Fig. 11 shows the human driver steering angle δ_{sw-h}, the *AFS* steering angle δ_{sw-c} and the different total steering angles of both controllers. One can notice, both controllers provide almost the similar steering angle. The two controllers are in conflict with the driver between 35s and 50s and between 70s and 85s in order to compensate his errors. As we can notice, oscillations appear more with the *STSM*-decentralized than the *LPV*$/\mathscr{H}_\infty$-centralized controller. Moreover, the advantage of using *STSM* control technique is that it is simple and easy to implement with a low cost. However, the point of weakness of this technique is the oscillation and chattering. Fig. 12 shows the braking of the *EMB* at the left and right rear wheels. The *LPV*$/\mathscr{H}_\infty$-centralized controller activates a little bit more the braking to compromise between the different objectives, on contrary to the *STSM*-decentralized controller which activates the braking only to cover back the lateral stability when necessary. Finally, Fig. 13 shows the longitudinal speed tracking to the desired one through a *STSM* longitudinal controller, the road curvature of the desired trajectory and finally the lateral and longitudinal accelerations. The lateral acceleration does not exceed the $\pm 5m/s^2$, and the actual longitudinal acceleration is pertinent ($< \pm 2m/s^2$) which demonstrate a comfortable and

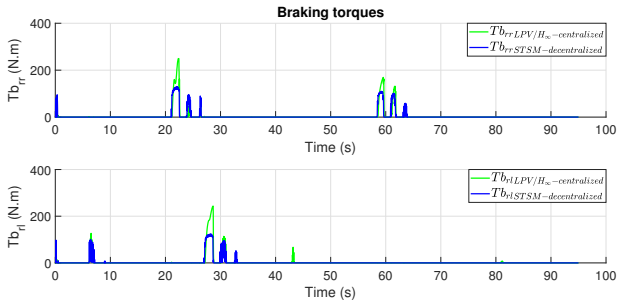

Fig. 12. The braking torques

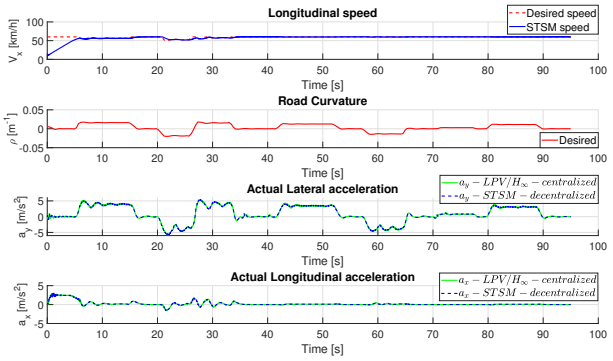

Fig. 13. The Vehicle dynamic variables

stable driving maneuver.

6. CONCLUSION AND PERSPECTIVES

To conclude, in this paper two *ADAS* system architectures have been developed involving the Active Front Steering (*AFS*) and the Direct Yaw Control (*DYC*) to assist the driver in the Lane Keeping maneuver and to enhance the lateral stability. The development of both *ADAS* controllers is done using the $LPV/\mathscr{H}_\infty$ and the Super-Twisting Sliding Mode (*STSM*) control techniques. The different layers including the decision layer for the decision making process are detailed. The proposed (*ADAS*) system architectures are validated in Matlab/Simulink for a given scenario with a complete nonlinear model of the vehicle, validated on "*SCANeR Studio*" (OKtal) simulator. In addition, a comparison between both control strategies is done. The results show the effectiveness and the performance of both approaches in terms of driver's error compensation and undesirable driving situation prevention. In the future work, we will consider other criteria to prove the performance of the decision making process and validate the approaches on the "*SCANeR Studio*" simulator, connected to a hardware-in-the-loop steering system.

REFERENCES

Apkarian, P. and Gahinet, P. (1995). A convex characterization of gain-scheduled $h\infty$ controllers. *IEEE Transactions on Automatic Control*, 40(5), 853–864.

Apkarian, P., Gahinet, P., and Becker, G. (1995). Self-scheduled $h\infty$ control of linear parameter-varying systems: a design example. *Automatica*, 31(9), 1251–1261.

Atoui, H., Milanés, V., Sename, O., and Martinez, J.J. (2021). Real-time look-ahead distance optimization for smooth and robust steering control of autonomous vehicles. In *2021 29th Mediterranean Conference on Control and Automation (MED)*, 924–929. IEEE.

Borroni, F. and Tanelli, M. (2018). A weighting approach to the shared-control of lateral vehicle dynamics. *IFAC-PapersOnLine*, 51(9), 305–310.

Doumiati, M., Sename, O., Dugard, L., Martinez-Molina, J.J., Gaspar, P., and Szabo, Z. (2013). Integrated vehicle dynamics control via coordination of active front steering and rear braking. *European Journal of Control*, 19(2), 121–143.

Doumiati, M., Victorino, A., Talj, R., and Charara, A. (2014). Robust lpv control for vehicle steerability and lateral stability. In *53rd IEEE Conference on Decision and Control, pp. 4113–4118*.

Favarò, F.M., Nader, N., Eurich, S.O., Tripp, M., and Varadaraju, N. (2017). Examining accident reports involving autonomous vehicles in california. *PLoS one*, 12(9), e0184952.

Hamdan, A., Chokor, A., Talj, R., and Doumiati, M. (2020). A centralized multilayer lpv/h-infinity control architecture for vehicle's global chassis control, and comparison with a decentralized architecture. In *21rst IFAC (International Federation of Automatic Control)*.

Hamdan, A., Talj, R., and Cherfaoui, V. (2021). A fuzzy logic shared steering control approach for semi-autonomous vehicle. In *2021 20th International Conference on Advanced Robotics (ICAR)*, 83–90. IEEE.

Kukkala, V.K., Tunnell, J., Pasricha, S., and Bradley, T. (2018). Advanced driver-assistance systems: A path toward autonomous vehicles. *IEEE Consumer Electronics Magazine*, 7(5), 18–25.

Li, A., Chen, Y., Lin, W.C., and Du, X. (2020). Shared steering control of tire blowout for ground vehicles. In *2020 American Control Conference (ACC)*, 4862–4867. IEEE.

Nguyen, A., Sentouh, C., and Popieul, J.C. (2015). Online adaptation of the authority level for shared lateral control of driver steering assist system using dynamic output feedback controller. In *IECON 2015-41st Annual Conference of the IEEE Industrial Electronics Society*, 003767–003772. IEEE.

Perozzi, G., Sentouh, C., Floris, J., and Popieul, J.C. (2020). On nonlinear control for lane keeping assist system in steer-by-wire road wheeled vehicles.

Scherer, C., Gahinet, P., and Chilali, M. (1997). Multiobjective output-feedback control via lmi optimization. *IEEE Transactions on automatic control*, 42(7), 896–911.

Sename, O., Gaspar, P., and Bokor, J. (2013). *Robust control and linear parameter varying approaches: application to vehicle dynamics*. Springer, vol. 437.

Sentouh, C., Soualmi, B., Popieul, J.C., and Debernard, S. (2013). Cooperative steering assist control system. In *2013 IEEE international conference on systems, man, and cybernetics*, 941–946. IEEE.

Soualmi, B., Sentouh, C., Popieul, J.C., and Debernard, S. (2011). Fuzzy takagi-sugeno lq controller for a shared control of vehicle. In *2011 14th International IEEE Conference on Intelligent Transportation Systems (ITSC)*, 956–961. IEEE.

Tan, H.S. and Huang, J. (2014). Design of a high-performance automatic steering controller for bus revenue service based on how drivers steer. *IEEE Transactions on Robotics*, 30(5), 1137–1147.

Zin, A. (2005). *Sur la commande robuste de suspensions automobiles en vue du contrôle global de châssis.* Ph.D. thesis, Institut National Polytechnique de Grenoble-INPG.